Single-cell analyses of CSF and PBMCs from anti-NMDAR encephalitis patients reveals distinct characteristics of T cell subpopulations

Sisi Li[1,2a], Xiang Hu[3a], Yi Yang[1], Jierui Wang[1], Zhen Hong[1], Dong Zhou[1*], Jinmei Li[1*]

[1] Department of Neurology, West China Hospital, Sichuan University, No. 37 Guoxue Road, Chengdu, Sichuan 610041, People's Republic of China

[2] Department of Breast Cancer, Chongqing University Cancer Hospital, Chongqing, 400030, China

[3] State Key Laboratory of Biotherapy, West China Hospital, Sichuan University, Chengdu, 610041, China

[a]These authors contributed equally to this work.

Corresponding author:

Jinmei Li, MD, Ph.D.

Department of Neurology, West China Hospital, Sichuan University

No. 37 Guoxue Road, Chengdu, Sichuan 610041, People's Republic of China

Email:lijinmei@wchscu.cn

Fax and Tel: 86-028-85422549

Dong Zhou, MD, Ph.D.

Department of Neurology, West China Hospital, Sichuan University

No. 37 Guoxue Road, Chengdu, Sichuan 610041, People's Republic of China\

Email: zhoudong66@yahoo.de

Fax and Tel: 86-028-85422549

Abstract

Background: Anti-N-methyl-D-aspartate receptor encephalitis (NMDAR-E) is a common and severe antibody-mediated autoimmune encephalitis. While the roles of B cells and NMDAR antibodies in NMDAR-E have been extensively studied, the involvement of T cell subpopulations in the disease progression remains unclear.

Methods: This study conducted single-cell RNA sequencing, single-cell TCR sequencing, and flow cytometry to analyze the T cell subpopulations and their transcriptomic characteristics in NMDAR-E patients and control individuals. Furthermore, it explored the interaction between $CD8^+$T cells and B cells through in vitro cell co-culture and cell communication analysis.

Results: The study found activated $CD8^+$T cell subpopulations in the cerebrospinal fluid (CSF) and peripheral blood mononuclear cells (PBMCs) of NMDAR-E patients, with some subpopulations exhibiting significant TCR clonal expansion. Differential expression gene analysis revealed upregulation of genes related to cytotoxicity, tissue residency, Th1, IFN, or TCR signaling in certain activated $CD8^+$T cell and $CD4^+$ memory T cell subpopulations. In vitro co-culture experiments demonstrated that $CD8^+$T cells from the PBMCs of NMDAR-E patients could induce apoptosis of their own B cells. Cell interaction analysis revealed the existence of interactions between KIR^+CD8^+T cells and B cell subpopulations in NMDAR-E patients.

Conclusion: This study explored the changes and transcriptomic characteristics of activated $CD8^+$T cell subpopulations in the CSF and PBMCs of NMDAR-E patients. Additionally, it discovered the impact of $CD8^+$T cells from NMDAR-E patients on their own B cells, providing new evidence for the interaction between $CD8^+$T cells and B cells.

Keywords: Anti-NMDA receptor encephalitis; single-cell RNA sequencing; single-cell TCR sequencing; $CD8^+$T cells; KIR^+CD8^+T cells

1.Introduction

Anti-N-methyl-D-aspartate receptor (NMDAR) encephalitis (NMDAR-E) is a recently discovered common autoimmune encephalitis (AE). It is caused by autoantibodies against the NMDAR NR1 subunit, leading to severe diffuse brain inflammation symptoms [1, 2], including psychiatric symptoms, cognitive impairments, seizures, complex movement disorders, or unexplained coma [3, 4]. Current first-line immune therapies include steroids, plasma exchange, and intravenous immunoglobulin, but approximately 20% of patients do not respond to these treatments [5-7]. Additionally, about 75% of patients require intensive care unit treatment [3, 8], and 20-25% are at risk of relapse [7, 8]. Due to the pathogenicity of NR1-IgG being established [9-11], the clinical use of anti-CD20 monoclonal antibodies (such as rituximab (RTX) and ocrelizumab (OFA)) in NMDAR antibody encephalitis is increasingly widespread, though their effectiveness is limited in some patients [12]. Furthermore, nearly all patients experience long-term sequelae, such as persistent cognitive deficits [13]. Despite extensive research into the pathogenic role of NR1-IgG autoantibodies in NMDAR-E, previous studies have primarily focused on B cell subsets, such as antibody-producing cells, with limited understanding of other immune cell subsets.

Recent studies have shown that T cell subsets may play a role in the pathogenesis of NMDAR-E. Studies have demonstrated significantly elevated levels of T cell-related cytokines in the cerebrospinal fluid (CSF) of NMDAR-E patients [14-16]. In brain tissue samples from these patients, infiltration of T cells around brain parenchyma and perivascular spaces has been observed [17-19]. Animal models of NMDAR-E have revealed infiltration of $CD4^+$ and $CD8^+$T cell subsets in critical brain regions [20]. In a mouse model of autoimmune encephalitis induced by repeated streptococcal infections, Th17 lymphocytes play a crucial role in the entry of autoantibodies into the central nervous system (CNS), sustained activation of microglia, and neurological deficits [21]. Another study established a humanized mouse model by transferring peripheral blood mononuclear cells (PBMCs) from NMDAR-E patients, showing infiltration of $CD8^+$T cells in the hippocampal region [22]. However, despite the observed infiltration of $CD8^+$T cells in brain tissues of NMDAR-E patients and animal models, no signs of neuronal apoptosis or necrosis have been found [17, 19], suggesting that $CD8^+$T cells may not attack neurons through

cytotoxic effects. Further exploration is needed to investigate whether $CD8^+$T cells play other roles in NMDAR-E.

CSF is a transparent fluid that envelops and protects the CNS, forming a unique local immune environment [23]. Under healthy conditions, the non-cellular components of CSF primarily consist of serum ultrafiltrate [23]. Clinically, CSF aids in the diagnosis of CNS inflammatory and degenerative diseases. However, the concentration of cells in CSF is approximately 1,000 times lower than in blood, and the volume that can be safely sampled from each patient is limited. Single-cell transcriptomics is a transformative and rapidly advancing technology primarily used to redefine the heterogeneity of complex tissues in healthy rodents or humans [24, 25]. However, its application in autoimmune encephalitis such as NMDAR-E is not yet widespread. To our knowledge, only three studies have reported the transcriptomic and immunological characteristics of B cell subsets in the CSF, peripheral blood (PB), and teratoma tissues of NMDAR-E patients [26-28]. To date, no studies have reported the transcriptomic and immunological characteristics of T cell subsets in CSF and PB of NMDAR-E patients.

Based on this, our study utilizes a combination of single-cell RNA sequencing (scRNA-seq), single-cell T cell receptor sequencing (scTCR-seq), flow cytometry, and in vitro co-culture methods to explore the phenotypes of T cells, TCR clonality, and the interactions between T cell subsets and B cells in NMDAR-E patients (Fig. 1A). This research aims to fill the current research gap regarding T cell subsets in NMDAR-E and provide new insights into the interactions between T cells and B cells.

2. Methods

2.1 Selection of Patients and Controls

All samples were collected from West China Hospital, Sichuan University between January 2021 and January 2023, and recruited patients met the diagnostic criteria for NMDAR-E[1]. The inclusion criteria for NMDAR-E in patients were consistent with our team's previous report[29]. This study obtained ethical approval from the Institutional Review Board (IRB) of West China Hospital (Protocol No. ChiCTR1900027074) and followed the ethical principles outlined in the Declaration of Helsinki. Exclusion criteria included: (1) patients with coexisting autoantibodies; (2) patients who have received late-stage immunotherapy

(such as Rituximab, OFA, cyclophosphamide, etc.); (3) patients who refused to participate.

Inclusion criteria for the CSF control group samples are as follows: (1) Negative results in CSF examination, including routine, biochemical, and IgG tests, as well as negative results for bacterial, fungal and viral tests; (2) Negativity for autoantibodies in the CSF, demyelinating antibodies, and antibodies associated with paraneoplastic syndromes; (3) No Signs of inflammation should be observed in the cranial magnetic resonance imaging (MRI); (4) Patients should be in good physical health; (5) The final diagnosis should be idiopathic intracranial hypertension, chronic headache, or other non-organic central nervous system diseases. The PBMCs control group samples are obtained from healthy adult volunteers matched for age and gender with the enrolled patients.

2.2 Sample information for single cell analysis and flow cytometry

This study investigated scRNA-seq and scTCR-seq analyses using samples from nine subjects, consisting of three CSF samples from NMDAR-E patients, four PBMC samples from NMDAR-E patients, and two PBMC samples from control individuals. In addition, six CSF control samples from idiopathic intracranial hypertension (IIH) were obtained from the public dataset GSE138266 and were used for scRNA-seq analysis (Table S1).

Flow cytometry was used to detect changes in T-cell subsets in the CSF and PBMC of patients with NMDAR-E as well as in the controls. The following analyses were conducted: (1) a total of 25 CSF samples (NMDAR-E, n=15; control, n=12) (Table S2) and 55 PBMCs (acute-phase NMDAR-E, n=34; relapse-phase NMDAR-E, n=13; controls, n=21) (Table S3); (2) $KIR^{+}CD8^{+}T$ cell subsets were analyzed in samples from 40 NMDAR-E (acute severe phase, n=9; acute mild/moderate phase, n=10; relapse-phase, n=13; remission-phase, n=8) as well as 11 controls (Table S4). Due to PBMCs samples separation into two batches for testing, the first batch only examined the $CD8^{+}$ and $CD4^{+}T$ cell subsets of the acute-phase and control group samples. In the second batch (as shown in Table S4), the $CD8^{+}$ and $CD4^{+}T$ cell subsets of the acute-phase, relapse-phase, and control group samples were simultaneously tested for $KIR^{+}CD8^{+}T$ cell subset. The analysis in Table S3 includes data from both the first and second batches.

Disease severity was assessed using the mRS scores [30], where a score of <3 indicated mild illness and ≥3 indicated moderate/severe illness. Relapse was defined as the recurrence

or emergence of new symptoms after a period of at least 2 months marked by clinical stabilization or improvement [31].

2.3 Collection and processing of CSF and PB samples

PB samples (4-5 mL) were obtained from both NMDAR-E patients and control groups. To isolate PBMCs, Ficoll-Paque medium (Ficoll Paque Plus, GE Healthcare) was used for density gradient centrifugation. After separation, PBMC samples were preserved by freezing them overnight at -80°C and subsequently transferring them to liquid nitrogen for long-term storage. These samples were later used for scRNA-Seq, scTCR-seq, and flow cytometry analysis.

We collected CSF samples from both NMDAR-E patients and control groups via lumbar puncture. Fresh CSF samples of 15-30 mL were required for scRNA-seq and scTCR-seq analysis, while 5-10 mL of fresh CSF samples were needed for flow cytometry analysis. Sample processing was conducted within 2 hours after collection. Fresh CSF samples were used for scRNA-Seq, scTCR-seq, and flow cytometry analysis.

2.4 Flow cytometry

PBMCs and CSF cells were suspended in phosphate-buffered saline (PBS) supplemented with 10% fetal calf serum (FCS). The cells were then treated for 30min with a mixture of antibodies. To characterize T cell subsets in CSF and PBMCs, the panel included the following antibodies: CD3-BV605, CD8-APC-Cy7, CD4-PerCP-Cy5-5, CD45RA-BV786, and CCR7-FITC. To analyze $KIR^{+}CD8^{+}T$ cells in PB, the following antibodies were used: CD3-BV605, CD8-APC-Cy7, CD45RA-BV786, CCR7-FITC, CD158b-PerCP-Cy5-5, and CD158e-PE. For the separation of $CD8^{+}T$ cells and B cells, the following antibodies were employed: CD3-BV605, CD8-APC-Cy7, 7AAD-PerCP-Cy5-5, and CD19-BV785. In vitro co-culture of $CD8^{+}T$ cells and B cells, as well as measurement of B cell apoptosis, were detected using the following antibodies: CD3-BV605, CD19-BV785, CD38-APC, CD27-PE-Cy7, IgD-APC-Cy7, AnnexinV-PE, and 7AAD-PerCp-Cy5-5. For each experiment, control samples were stained separately and left unstained. Flow cytometry experiments were performed using the LSRFortessa flow cytometer from BD Biosciences. A compensation matrix was developed to facilitate analysis using FlowJo software (v. 10.5.3, FlowJo LLC, BD). Detailed information for each flow cytometry antibody can be found in Table S5.

2.5 Single-cell RNA-Seq data analysis

Data processing, quality control, and batch correction strategies

The raw data underwent processing utilizing CellRanger software (version 7.0.0) and aligned with the GRCh38 human reference genome. The gene-barcode matrix was analyzed using Seurat package in R (version 4.2.0). During the quality control process, cells with less than 200 detected genes for environmental RNA, cells with mitochondrial gene expression total exceeding 15% for dead cells, and doublets identified by Scrublet (Python 3.7.3) were excluded. In order to mitigate the impact of batch effects, the single-cell variational inference (scVI) method was employed to integrate expression data from different samples [32]. ScVI is a powerful deep generation model that can learn the transcriptional state of a single cell and implicitly correct the batch effect [33].

Identification of cell cluster

To perform principal component analysis (PCA), we utilized Seurat's RunPCA function to select the top 2000 features displaying the most significant expression differences between cells. Subsequently, cell clustering was performed on the top 30 dimensions using the FindClusters function. The resulting clusters were visualized using t-distributed stochastic neighbor embedding (t-SNE), and the identification of cell types within each cluster was determined based on characteristic marker genes.

Cell clustering analysis

For the T/NK cell subclustering analysis, we utilized t-tests and beta-binomial generalized linear models from the aod::betabin package. These methods allowed us to examine differences in cluster abundance, measured as cell counts, between NMDAR-E encephalitis and control donors[33].

DEGs and pathway analysis

To identify genes exhibiting differential expression (DEGs), we employed Seurat's "FindMarkers" or "FindAllMarkers" functions. In addition, we utilized the Wilcoxon test to assess the significance of gene expression differences. Genes expressed in at least 25% of the cells within the target cluster were considered, and a p-value threshold below 0.05 was used to determine statistical significance. To visualize the expression patterns of specific genes, we generated violin plots using the Seurat package. Furthermore, for the enrichment analysis of

the identified DEGs in the Kyoto Encyclopedia of Genes and Genomes (KEGG), we utilized the singleseqgset package (https://github.com/arc85/singleseqgset).

Cell communication

To investigate the intercellular interactions between $KIR^{+}CD8^{+}T$ cell and B cell clusters in NMDAR-E patients and controls, we employed the R package CellChat. This package facilitated the identification and visualization of intercellular communication by leveraging known ligand-receptor pairs [34]. The CellChat package can be accessed at https://github.com/sqjin/CellChat. To explore the interactions between potential ligands and receptors, we analyzed the relative expression levels across different cell types using CellPhoneDB (v3.0.1) (www.CellPhoneDB.org). Heatmaps and bubble plots were generated using the ktplots (v1.2.1) R package to visualize these interactions.

2.6 Analysis of single-cell TCR sequencing data

The study utilized Cell Ranger software (version 6.0.1) to identify CDR3 sequences and rearranged TCR genes in the 10x Genomics dataset. The α-β pairing within the framework was considered to determine the dominant TCRs and unique clone types. Clonal populations were denoted by the presence of a clone type in at least two cells, and clonality was determined by the number of cells with the same dominant α-β pairing. Clonotypes were divided into three groups based on the number of T cells expressing the same TCR: ">=3", "2", and "1". Following a similar approach as described in previous studies[35, 36], we employed a statistical method to assess the sharing of TCR clones based on TCR clonotypes between different clusters. Specifically, to evaluate the sharing of TCR clones in both the NMDAR-E patient CSF and PB datasets, we generated a table for each pair of clusters and computed the number of clone types shared among cells within the same cluster or across different clusters.

2.7 In vitro experiments

The PBMCs of NMDAR-E patients and controls were prepared, and $CD8^{+}T$ cells and B cells were sorted by flow cytometry and co-cultured at a ratio of $CD8^{+}T$: B cells (5:1). After 1day and 7 days of cultivation, flow cytometry antibody staining was performed, incubated at 4□ in the dark for half an hour, then washed, resuspended, and filtered into flow tubes. The LSRFortessa flow cytometer (BD Biosciences) was used for detection.

2.8 Statistical analysis

Descriptive analysis was performed to examine the sociodemographic and clinical data, and the results were expressed as percentages or means using IBM SPSS Statistics version 22.0 (IBM Corp., Armonk, NY, USA). The flow cytometry analysis was conducted using FlowJo software (v. 10.5.3, FlowJo LLC, BD), and the graphs were generated using GraphPad Prism (V.9.0). To assess the differences between two cell subpopulations, an unpaired t-test was employed, while the differences among multiple groups were evaluated using the One-Way ANOVA test. To facilitate image layout, we utilized the commercial software Adobe Illustrator 2020. We described sample sizes and statistical tests methods in the figure legends to provide a comprehensive understanding of the results. Unless otherwise specified, P-values or adjusted P-values less than 0.05 were considered significant.

3. Results

3.1 Composition and signature marker genes of T/NK cell subsets

After conducting quality control and technical noise adjustment, a total of 45,088 single-cell transcriptomic profiles were included for analysis (Table S6). Additionally, we incorporated 14,536 CSF cells from six idiopathic intracranial hypertension (IIH) patients obtained from a publicly available database as control samples (GSE138266). Detailed gene expression levels for each group can be found in Figure S1A. Through the utilization of t-SNE and assessment of the expression of characteristic marker genes, we thereby classified 59,624 single cells into eight immune cell clusters (Figure S1B-S1D). Our previous research had elucidated B cell phenotypes in the CSF and PB of NMDAR-E patients [28]. This study primarily focuses on investigating the composition of T cell subpopulations and transcriptomic changes.

In this study, the total number of T/NK cells analyzed from the CSF and PB of NMDAR-E patients and controls was 47,922 (Figure 1B). To classify different T/NK cell subsets, we used marker genes and identified distinct clusters (Figure 1C and 1D). $CD4^+$T cells were divided into two groups. Naïve $CD4^+$T cells ($CD4^+$Tn) exhibited high expression of *CCR7*, *SELL*, and *LEF1* genes, while memory $CD4^+$T cells ($CD4^+$Tm) demonstrated low expression of these genes. $CD8^+$T cell subsets were divided into non-activated $CD8^+$T ($CD8^+$Tna) cells and activated $CD8^+$T ($CD8^+$Ta) cells. $CD8^+$Tna cells exhibited high expression of *CCR7*, *SELL*, and *LEF1*. $CD8^+$Ta cells consisted of three groups, where the first ($CD8^+$Ta_1) and

third ($CD8^+$Ta_3) groups highly expressed *CD8B* and *GZMK* genes and were biased towards the characteristics of effector memory $CD8^+$T ($CD8^+$Tem) cells, while the second group ($CD8^+$Ta_2) highly expressed *GZMH*, *GNLY*, *PRF1*, *GZMB* genes and exhibited similar features to that of effector $CD8^+$T cells [37]. In addition, we also identified gdT (*TRDV2* and *TRGV9*), Treg (*Foxp3* and *CTLA4*), MAIT (*SLC4A10*), and NK (*GNLY* and *NKG7*) cell subsets [33, 37].

The proportion of T cell subsets in the CSF and PB differs in NMDAR-E patients. In PB, $CD4^+$Tn, $CD8^+$Tna, and NK cells are predominant, while in CSF, $CD4^+$Tm and $CD8^+$Ta cells are predominantly found (Figure S1E). In NMDAR-E patients, the proportion of the $CD8^+$Ta_1 subset is higher in PB than in the control group, whereas the proportions of $CD8^+$Ta_2 and $CD8^+$Ta_3 cell subsets are higher in CSF compared to the control group (Figure 1E). Additionally, we conducted flow cytometry analysis on $CD8^+$T and $CD4^+$T cell subsets in the CSF and PBMCs of patients with NMDAR-E and control subjects (Figure S2A). The results revealed a significant increase in the number of $CD45RA^+$effector memory $CD8^+$T cells ($CD8^+$Temra) in the CSF of NMDAR-E patients (Figure 1F). In PB, the levels of $CD8^+$Temra and $CD8^+$Tem cells were both significantly higher in the acute-phase and relapse-phase NMDAR-E patients compared to the control group (Figure 1G). There were no statistically significant differences in the levels of $CD4^+$T cell subsets between the two groups in PB and CSF (Figure S2B and S2C).

3.2 Transcriptome characteristics of T cell subsets

Through the analysis of the differential expression genes (DEGs) of T cell subpopulations in NMDAR-E patients and controls, the results showed that the $CD8^+$Ta cell subpopulation in the CSF and PB of NMDAR-E patients upregulated DEGs related to cytotoxicity compared to the control group (mainly *GZMK*, *PRF1*, and *GZMA* in CSF, and *GZMH* and *NKG7* in PB) [38, 39] (Figure 2). The $CD8^+$Ta_1, $CD8^+$Ta_2, and $CD4^+$Tm cell subpopulations in NMDAR-E CSF upregulated DEGs related to tissue residence (such as *CD69*, *CXCR6*, *PRDM1*, *LGALS3*) [38] (Figure 2A and 2B). In addition, compared to the control group, $CD4^+$Tm, $CD8^+$Ta, and gdT cells in the CSF and PB of NMDAR-E patients were found to upregulate DEGs related to co-inhibitory (such as *CTLA4*, *LAG3*, *ANXA1*), Th1-related genes (such as *TBX21*, *CXCR3*, *RUNX3*), interferon (IFN)-related genes (such as

IFNGR1, *IRF7*, *STAT1*), as well as T cell receptor (TCR) signaling pathway (such as *DUSP2*, *GIMAP1*, *GIMAP5*, *PIK3R1*) [36] (Figure 2). Furthermore, this difference was more pronounced in the CSF of NMDAR-E patients.

3.3 TCR clonal characteristics of T cell subsets

Through single-cell TCR sequencing, we observed that compared to the control group, NMDAR-E patients had a higher proportion of T cells with TCR clonotypes in PB, and this phenomenon was more pronounced in the patients' CSF (Figure 3A and 3B). T cell subpopulations with high TCR clonality (TCR clonotypes ≥3) were mainly distributed in $CD8^+$Ta_1, $CD8^+$Ta_2, $CD4^+$Tm, and MAIT cell subgroups, while the TCR clonality of $CD4^+$Tn and $CD8^+$Tn cells showed no pronounced changes (Figure 3C-3E). In the CSF of NMDAR-E patients, T cells with TCR clonality showed upregulation of cytotoxicity-related genes (such as *GZMA*, *GZMK*) [39] and cell migration-related genes (such as *CCL5*, *CCL4*, *CCL4L2*, *ITGB1*) [40], while genes related to naïve/memory status (such as *CCR7*, *SELL*) were downregulated (Figure 3G). Similarly, T cells with TCR clonality in the PB of NMDAR-E patients showed upregulation of DEGs related to cytotoxicity (such as *GZMH*, *GZHB*, *PRF1*) and cell migration (such as *CX3CR1*, *ITGB1*) [40] (Figure 3F and 3H). Moreover, we identified numerous shared TCR clonotypes in T cell subpopulations in the CSF and PB of NMDAR-E patients (Figure 3I and 3J). For instance, shared TCR sequences were observed between $CD4^+$Tn and $CD8^+$Tn in PB, and between $CD4^+$Tn and $CD4^+$Tm, as well as between $CD4^+$Tm and $CD8^+$Tem in the CSF, indicating a common clonal origin among these subpopulations.

3.4 In vitro co-cultured of $CD8^+$T and B cells

To explore the interaction between $CD8^+$T cells and B cells in NMDAR-E, we isolated PBMCs from both NMDAR-E patients and control individuals, and sorted $CD8^+$T cells and $CD19^+$B cells for co-culture. On the first day of co-culture, flow cytometry analysis indicated no significant difference in the apoptosis rate of $CD8^+$T and B cells between the control group and the NMDAR-E group (Figure 4A, 4B and 4D). However, on the 7th day of co-culture, apoptosis detection revealed a significantly higher apoptosis rate of B cells in the NMDAR-E group compared to the control group, while the apoptosis rate of $CD8^+$T cells showed no significant difference between them (Figure 4C and 4E). Specifically, the apoptosis proportions of antibody-secreting cells (ASCs), memory B cells (Bm), $CD27^-$ B cells, and

$CD27^-IgD^-$ double negative B (DN) cells in the NMDAR-E group were significantly higher than those in the control group (Figure 4F-4I). These results suggest a potential interaction between $CD8^+$T cells and B cells in NMDAR-E patients, leading to the apoptosis of B cell subpopulations.

3.5 Alteration of KIR^+CD8^+T cells in NMDAR-E

Previous research has indicated the presence of a regulatory subset of KIR^+CD8^+T cells within the $CD8^+$T cell population, characterized by high expression of Killer cell immunoglobulin-like receptor (KIR) genes. To explore this $CD8^+$T cell subsets, we analyzed the expression of KIRs in $CD8^+$T cells. The results revealed higher expression of *KIR3DL1* and *KIR2DL3* in $CD8^+$T cells in the CSF and PB of NMDAR-E patients compared to the control group, and these KIR^+CD8^+T cells were predominantly composed of activated $CD8^+$T cells (Figure 5A-5C). Further flow cytometry analysis of KIR^+CD8^+T cells in the PB of NMDAR-E patients and the control group revealed a higher level of $CD158b^-CD158e^+CD8^+$T (KIR^+CD8^+T) cells in the severe group compared to the control group (Figure 5D and 5E). Additionally, we observed a significant increase in the level of $CD45RA^+CCR7^-CD158b^-CD158e^+CD8^+$T ($KIR^+CD8^+$Temra) cells in relapse-phase NMDAR-E patients (Figure 5F).

3.6 TCR clonal characteristics of KIR^+CD8^+T and their interaction with B cells

scTCR-seq analysis revealed clonal expansion of KIR^+CD8^+T cells in both the CSF and PB of NMDAR-E patients (Figure 6A and 6B). Compared to KIR^+CD8^+T cells without TCR clonality, those with TCR clonality in the CSF and PB of NMDAR-E patients upregulated DEGs associated with NK cells (such as *KLRF1*, *KLRD1*, *KLRB1*) and were enriched in the natural killer cell-mediated cytotoxicity pathways (Figure 6C-6G). Additionally, KIR^+CD8^+T cells with TCR clonality in the PB of NMDAR-E patients upregulated genes related to cytotoxicity while downregulating genes associated with naive/memory markers (Figure 6C and 6E).

Cell interaction analysis indicated stronger interactions between KIR^+CD8^+T cells from the CSF and PB of NMDAR-E patients with naive B cells (Bn) and memory B cells (Bm) compared to the control group (Figure 6H). Further receptor-ligand pairing analysis demonstrated interactions between KIR genes (including *KIR3DL1*, *KIR2DL3*, and *KIR2DL1*) and NK-related molecules (*KLRC2* and *KLRK1*) expressed on KIR^+CD8^+T cells from the CSF

and PB of NMDAR-E patients, and MHC-I molecules (including *HLA-A*, *HLA-C*, and *HLA-E*) expressed on B cells (Figure 6I).

4. Discussion

This study used scRNA-seq, scTCR-seq, and flow cytometry to analyze changes in T cell subpopulations, transcriptional features, and immune characteristics in NMDAR-E patients for the first time. Additionally, we observed that $CD8^+$T cells from NMDAR-E patients promoted apoptosis of their own B cells, providing direct evidence for the connection between $CD8^+$T cells and B cells, and offering new insights into the role of T cell subsets in the pathogenesis of NMDAR-E.

Despite previous research on NMDAR-E primarily focusing on the roles of B cells and autoantibodies, there is increasing attention on the role of T cells in autoimmune encephalitis [41]. The cytokine/chemokine profile of human NMDAR-E cases in CSF supports evidence for T cell involvement [14, 15, 42, 43] . Currently, only a few studies have reported histopathological changes in NMDAR-E patients, with some cases showing immune cell infiltration and neuroinflammation [9, 17, 44, 45]. For example, one report noted the absence of plasma cells and B cells in brain tissue but persistent infiltration of $CD4^+$ and $CD8^+$ T cells following ineffective treatment with plasma exchange and rituximab [44]. Another report described NMDAR antibody-positive paraneoplastic encephalitis associated with SCLC, where cytotoxic T cells positive for CD3, CD8, TIA-1, and granzyme B were widely distributed in brain parenchyma [45]. However, there are also reports where T cell infiltration in brain tissue was not prominent [18], possibly influenced by timing and location of sample collection, reflecting individual variability. Although NMDAR-E mouse models show significantly higher average infiltration density of $CD4^+$ and $CD8^+$ T cells in the hippocampus six weeks post-immunization compared to controls [20], studies using antigen-reactive T cell enrichment techniques have found lower frequencies of CD154-expressing NR1-reactive $CD4^+$ helper T cells in NMDAR-E patients compared to healthy controls [46]. Therefore, research on T cell subsets in NMDAR-E remains limited, and their exact roles and alterations in disease mechanisms require further investigation. This study employed scRNA-seq and flow cytometry analysis, revealing no significant overall changes in the proportion of $CD4^+$ and $CD8^+$ T cells in CSF and PB of NMDAR-E patients compared to controls, but a significantly higher proportion of activated $CD8^+$T cell subsets, particularly $CD8^+$Temra cells, in recurrent NMDAR-E patients' PB

compared to controls and acute phase group. These findings suggest that beyond overall $CD8^+$T cell infiltration, specific $CD8^+$T cell subsets and their transcriptomic characteristics warrant further exploration to elucidate their roles in NMDAR-E.

After understanding the changes in T cell subpopulations in the CSF and PB of NMDAR-E patients, this study analyzed the transcriptional features of different T cell subpopulations using scRNA-seq. We observed that activated $CD8^+$T cell subpopulations (such as $CD8^+$Ta_1 and $CD8^+$Ta_2) in NMDAR-E patient CSF, as well as $CD4^+$Tm subpopulations, expressed tissue-resident related genes like *CD69* and *CXCR6*. *CD69*, a major phenotypic marker of tissue-resident memory T cells (Trm), is a transmembrane glycoprotein that can influence T cell migration by downregulating S1PR1 expression [47]. Trm cells have the ability to secrete pro-inflammatory cytokines and attract other leukocytes [48]. Additionally, *CXCR6* is also a characteristic marker of Trm cells [49, 50]. In the CNS, the CXCL16/CXCR6 signaling pathway regulates the number of $CD8^+$Trm cells and plays a role in their interaction with microglial cells [49]. Furthermore, DEGs showed higher expression of *CXCR3* (the receptor for chemokines CXCL9 and CXCL10) in $CD4^+$ and $CD8^+$T cell subpopulations in NMDAR-E patient CSF. *CXCR3* plays a crucial role in the development of Trm cells [51]. Several studies have reported an increase in CXCL10 cytokine levels in the CSF of NMDAR-E patients [15, 16, 52]. Therefore, the tissue-resident characteristics expressed by T cell subpopulations in NMDAR-E may influence their migratory capabilities or recruit other leukocytes (such as B cell subpopulations) to infiltrate the CNS through the secretion of inflammatory cytokines.

In addition, we observed that T cell subsets (including $CD4^+$Tm, $CD8^+$Ta, and gdT cells) in the CSF and PB of NMDAR-E patients exhibit elevated expression of characteristic genes associated with TH1 cells, such as *TBX21* and *CXCR3*. TH1 cells can secrete cytokines like IFN-γ, TNF-α, IL-2, GM-CSF, promoting T cell proliferation, differentiation, and maturation [53]. Previous studies have also reported significant elevation of TH1 axis cytokines in the CSF of NMDAR-E patients, including IFN-γ [15], CXCL10 [15, 16, 52], and TNF-α [15, 52, 54]. Furthermore, T cell subsets in the CSF of NMDAR-E patients show upregulation of IFN-related genes, including *IFNGR1*, *IRF7*, and *STAT1*. *IRF7*, as a member of the interferon regulatory factor family, activates the JAK-STAT

pathway, inducing the expression of type I interferon genes, thereby enhancing the production of antiviral proteins, demonstrating robust antiviral functionality [55]. Type II interferon (IFN-γ), upon binding with its receptor complex (IFNGR1 and IFNGR2), primarily stimulates the maturation and differentiation of immune cells via STAT1 activation, thereby enhancing adaptive immune responses, demonstrating superior immune regulatory effects [56]. In summary, activation of the TH1 and IFN-related pathways in T cells of NMDAR-E patients may promote the maturation and differentiation of immune cells, playing a potential role in immune regulation.

Upon recognition of homologous antigens, $CD8^+$T cells undergo rapid clonal expansion and differentiate into effector and memory cells [57]. Our study identified some subsets of effector $CD8^+$T and $CD4^+$Tm cells in the CSF and PB of NMDAR-E patients exhibiting TCR clonality. DEGs analysis revealed that these $CD8^+$T cells with TCR clonality possess potential cytotoxic and chemotactic properties. Studies in CNS diseases such as multiple sclerosis [58], Parkinson's disease [59], and Alzheimer's disease [39] have also reported TCR expansions. For instance, in Alzheimer's disease, autoreactive cytotoxic T cells can recognize self-antigens, leading to target cell death and exacerbating neuroinflammation [39]. Further investigation into the role of autoreactive $CD8^+$T cells in CNS diseases is warranted. For example, identifying TCR sequences specific to NMDA autoantigens could enhance our understanding of the pathogenesis of NMDAR-E and lay the groundwork for developing new diagnostic and therapeutic approaches.

Interesting findings from this study revealed that $CD8^+$T cells from NMDAR-E patients can promote apoptosis of their own B cells, suggesting an interaction between $CD8^+$T cells and B cells in NMDAR-E encephalitis. Although traditionally most $CD8^+$T cells are thought to be involved in controlling infections caused by pathogens or targeting cancer cells, emerging evidence suggests that there is a subset of $CD8^+$T cells with the function of regulating the self-immune response[60]. Human KIR^+CD8^+T cells function similarly to the immune-suppressive subset $Ly49^+CD8^+$T cells in mice, increasing in certain autoimmune or infectious diseases (e.g., celiac disease, multiple sclerosis, COVID-19), and maintaining immune tolerance by suppressing excessive activation of immune cells [40, 61-63]. In NMDAR-E, the cytotoxic effect of $CD8^+$T cells on self-B cells may be attributed to these regulatory $CD8^+$T cell subsets, which can mediate B cell apoptosis. This study

found that the transcriptional characteristics of KIR^+CD8^+T cells in NMDAR-E are consistent with the findings of Li et al.[40]. Cell interaction analysis indicated that B cells in the CSF and PB of NMDAR-E patients express various MHC-I molecules, which interact with KIR^+CD8^+T cells through receptor-ligand interactions. Li et al. demonstrated that human KIR^+ $CD8^+T$ cells can kill pathogenic $CD4^+T$ cells via MHC-I molecules [40]. Similarly, mouse $Ly49^+$ $CD8^+T$ cells depend on perforin and classical/non-classical MHC-I molecules [64]. Therefore, there may exist a subset of $CD8^+T$ cells in NMDAR-E that regulate immune responses by modulating the cytotoxicity against self-B cells, although the specific mechanisms require further exploration.

Our study has several limitations. Firstly, we used publicly available databases as controls for CSF, which may introduce potential batch effects. To mitigate this, we employed scVI methods for data analysis to enhance the reliability and validity of our findings. Secondly, cell communication analysis revealed interactions between KIR^+CD8^+T cells and B cell subsets. However, due to the very low numbers of KIR^+CD8^+T cells in clinical samples, it was challenging to isolate a sufficient quantity from CSF or PBMCs for further study. Lastly, our study samples were derived from NMDAR-E patients' CSF and PB. While this method reflects the actual disease state directly, it also limits the depth of our investigation. Future research could involve establishing an NMDAR-E mouse model to delve deeper into the roles and mechanisms of T cell subsets in NMDAR-E.

Conclusion

This study found that the proportion of activated $CD8^+T$ cell subsets in the CSF and PB of NMDAR-E patients is elevated, accompanied by TCR clonality. Differential gene expression analysis revealed upregulation of genes related to cytotoxicity, tissue residency, Th1, IFN, or TCR signaling in some activated $CD8^+T$ cell and $CD4^+T$ memory cell subsets. In vitro co-culture experiments demonstrated that $CD8^+T$ cells from PB of NMDAR-E patients can promote apoptosis of their own B cells. Further cell interaction analysis revealed interactions between KIR^+CD8^+T cells and B cell subsets in NMDAR-E patients. However, whether KIR^+CD8^+T cells mediate apoptosis of their own B cells in NMDAR-E requires further exploration. Overall, this study suggests that $CD8^+T$ cell subsets may participate in the pathogenesis of NMDAR-E by

influencing B cell subsets, offering potential value for exploring new therapeutic approaches in the future.

Acknowledgment

This work was supported by grants from Chongqing Natural Science Foundation (Grant No. 2024NSCQ-MSX0894), National Science Foundation of China (Grant No. 81571272 and 82071459), and the 1.3.5 project for disciplines of excellence and Brain Science project of West China Hospital, Sichuan University (Grant No. ZYJC21001). The authors express their gratitude to Genenergy Shanghai for their support, as well as to all the patients who generously participated in the study. Thanks to Dr. Yuan Liang for his help in our data analysis.

Author contributions

JL and DZ designed this study and revised the final version of the draft. SL and XH carried out this study; those authors collected samples, analyzed data, wrote the draft, and contributed equally to this study; YY, and JW assisted in collecting the samples; ZH edited the manuscript.

Declarations of interest

The authors declare no disclosures relevant to the manuscript.

Data availability statement

The raw sequence data reported in this article are currently being uploaded to the Genome Sequence Archive (GSA: PRJCA014916) at the National Genomics Data Center, Beijing Institute of Genomics, Chinese Academy of Sciences. Once the upload is complete, these data will be publicly accessible at https://ngdc.cncb.ac.cn/gsa. Currently, interested parties can request access to the relevant data by contacting the corresponding author. The data sets supporting the conclusions of this article are included within the article and its accompanying files.

References

1. Graus F, Titulaer MJ, Balu R, et al. A clinical approach to diagnosis of autoimmune encephalitis. The Lancet Neurology 2016;15:391-404.

2. Gleichman AJ, Spruce LA, Dalmau J, Seeholzer SH, Lynch DR. Anti-NMDA receptor encephalitis antibody binding is dependent on amino acid identity of a small region within the GluN1

amino terminal domain. J Neurosci 2012;32:11082-11094.

3. Dalmau J, Lancaster E, Martinez-Hernandez E, Rosenfeld MR, Balice-Gordon R. Clinical experience and laboratory investigations in patients with anti-NMDAR encephalitis. The Lancet Neurology 2011;10:63-74.

4. Dalmau J, Armangué T, Planagumà J, et al. An update on anti-NMDA receptor encephalitis for neurologists and psychiatrists: mechanisms and models. The Lancet Neurology 2019;18:1045-1057.

5. Titulaer MJ, McCracken L, Gabilondo I, et al. Treatment and prognostic factors for long-term outcome in patients with anti-NMDA receptor encephalitis: an observational cohort study. The Lancet Neurology 2013;12:157-165.

6. Xu X, Lu Q, Huang Y, et al. Anti-NMDAR encephalitis: A single-center, longitudinal study in China. Neurol Neuroimmunol Neuroinflamm 2020;7.

7. Gable MS, Sheriff H, Dalmau J, Tilley DH, Glaser CA. The frequency of autoimmune N-methyl-D-aspartate receptor encephalitis surpasses that of individual viral etiologies in young individuals enrolled in the California Encephalitis Project. Clin Infect Dis 2012;54:899-904.

8. Prüss H, Dalmau J, Harms L, et al. Retrospective analysis of NMDA receptor antibodies in encephalitis of unknown origin. Neurology 2010;75:1735-1739.

9. Tüzün E, Zhou L, Baehring JM, Bannykh S, Rosenfeld MR, Dalmau J. Evidence for antibody-mediated pathogenesis in anti-NMDAR encephalitis associated with ovarian teratoma. Acta neuropathologica 2009;118:737-743.

10. Kreye J, Wenke NK, Chayka M, et al. Human cerebrospinal fluid monoclonal N-methyl-D-aspartate receptor autoantibodies are sufficient for encephalitis pathogenesis. Brain 2016;139:2641-2652.

11. Wenke NK, Kreye J, Andrzejak E, et al. N-methyl-D-aspartate receptor dysfunction by unmutated human antibodies against the NR1 subunit. Ann Neurol 2019;85:771-776.

12. Thaler FS, Zimmermann L, Kammermeier S, et al. Rituximab Treatment and Long-term Outcome of Patients With Autoimmune Encephalitis: Real-world Evidence From the GENERATE Registry. Neurol Neuroimmunol Neuroinflamm 2021;8.

13. Heine J, Kopp UA, Klag J, Ploner CJ, Prüss H, Finke C. Long-Term Cognitive Outcome in Anti-N-Methyl-D-Aspartate Receptor Encephalitis. Ann Neurol 2021;90:949-961.

14. Byun JI, Lee ST, Moon J, et al. Distinct intrathecal interleukin-17/interleukin-6 activation in anti-N-methyl-d-aspartate receptor encephalitis. J Neuroimmunol 2016;297:141-147.

15. Liba Z, Kayserova J, Elisak M, et al. Anti-N-methyl-D-aspartate receptor encephalitis: the clinical course in light of the chemokine and cytokine levels in cerebrospinal fluid. J Neuroinflammation 2016;13:55.

16. Liu J, Liu L, Kang W, et al. Cytokines/Chemokines: Potential Biomarkers for Non-paraneoplastic Anti-N-Methyl-D-Aspartate Receptor Encephalitis. Front Neurol 2020;11:582296.

17. Camdessanche JP, Streichenberger N, Cavillon G, et al. Brain immunohistopathological study in a patient with anti-NMDAR encephalitis. Eur J Neurol 2011;18:929-931.

18. Bien CG, Vincent A, Barnett MH, et al. Immunopathology of autoantibody-associated encephalitides: clues for pathogenesis. Brain 2012;135:1622-1638.

19. Martinez-Hernandez E, Horvath J, Shiloh-Malawsky Y, Sangha N, Martinez-Lage M, Dalmau J. Analysis of complement and plasma cells in the brain of patients with anti-NMDAR encephalitis. Neurology 2011;77:589-593.

20. Jones BE, Tovar KR, Goehring A, et al. Autoimmune receptor encephalitis in mice induced

by active immunization with conformationally stabilized holoreceptors. Sci Transl Med 2019;11.

21. Platt MP, Bolding KA, Wayne CR, et al. Th17 lymphocytes drive vascular and neuronal deficits in a mouse model of postinfectious autoimmune encephalitis. Proc Natl Acad Sci U S A 2020;117:6708-6716.

22. Shu Y, Peng F, Zhao B, et al. Transfer of patient's peripheral blood mononuclear cells (PBMCs) disrupts blood-brain barrier and induces anti-NMDAR encephalitis: a study of novel humanized PBMC mouse model. J Neuroinflammation 2023;20:164.

23. Engelhardt B, Carare RO, Bechmann I, Flügel A, Laman JD, Weller RO. Vascular, glial, and lymphatic immune gateways of the central nervous system. Acta neuropathologica 2016;132:317-338.

24. Macosko EZ, Basu A, Satija R, et al. Highly Parallel Genome-wide Expression Profiling of Individual Cells Using Nanoliter Droplets. Cell 2015;161:1202-1214.

25. Klein AM, Mazutis L, Akartuna I, et al. Droplet barcoding for single-cell transcriptomics applied to embryonic stem cells. Cell 2015;161:1187-1201.

26. Jiang Y, Dai S, Jia L, et al. Single-cell transcriptomics reveals cell type-specific immune regulation associated with anti-NMDA receptor encephalitis in humans. Front Immunol 2022;13:1075675.

27. Al-Diwani A, Theorell J, Damato V, et al. Cervical lymph nodes and ovarian teratomas as germinal centres in NMDA receptor-antibody encephalitis. Brain 2022.

28. Li S, Hu X, Wang M, et al. Single-cell RNA sequencing reveals diverse B cell phenotypes in patients with anti-NMDAR encephalitis. Psychiatry Clin Neurosci 2023.

29. Li S, Hu X, Wang M, et al. Single-cell RNA sequencing reveals diverse B cell phenotypes in patients with anti-NMDAR encephalitis. Psychiatry Clin Neurosci 2024;78:197-208.

30. Balu R, McCracken L, Lancaster E, Graus F, Dalmau J, Titulaer MJ. A score that predicts 1-year functional status in patients with anti-NMDA receptor encephalitis. Neurology 2019;92:e244-e252.

31. Macher S, Zrzavy T, Hoftberger R, et al. Longitudinal measurement of cerebrospinal fluid neurofilament light in anti-N-methyl-D-aspartate receptor encephalitis. Eur J Neurol 2021;28:1401-1405.

32. Lopez R, Regier J, Cole MB, Jordan MI, Yosef N. Deep generative modeling for single-cell transcriptomics. Nat Methods 2018;15:1053-1058.

33. Schafflick D, Xu CA, Hartlehnert M, et al. Integrated single cell analysis of blood and cerebrospinal fluid leukocytes in multiple sclerosis. Nat Commun 2020;11:247.

34. Jin S, Guerrero-Juarez CF, Zhang L, et al. Inference and analysis of cell-cell communication using CellChat. Nat Commun 2021;12:1088.

35. Luoma AM, Suo S, Williams HL, et al. Molecular Pathways of Colon Inflammation Induced by Cancer Immunotherapy. Cell 2020;182:655-671.e622.

36. Luoma AM, Suo S, Wang Y, et al. Tissue-resident memory and circulating T cells are early responders to pre-surgical cancer immunotherapy. Cell 2022.

37. Zhang L, Yu X, Zheng L, et al. Lineage tracking reveals dynamic relationships of T cells in colorectal cancer. Nature 2018;564:268-272.

38. Pappalardo JL, Zhang L, Pecsok MK, et al. Transcriptomic and clonal characterization of T cells in the human central nervous system. Sci Immunol 2020;5.

39. Gate D, Saligrama N, Leventhal O, et al. Clonally expanded CD8 T cells patrol the cerebrospinal fluid in Alzheimer’s disease. Nature 2020;577:399-404.

40. Li J, Zaslavsky M, Su Y, et al. KIR(+)CD8(+) T cells suppress pathogenic T cells and are

active in autoimmune diseases and COVID-19. Science 2022;376:eabi9591.

41. Pilli D, Zou A, Tea F, Dale RC, Brilot F. Expanding Role of T Cells in Human Autoimmune Diseases of the Central Nervous System. Front Immunol 2017;8:652.

42. Ulusoy C, Tüzün E, Kürtüncü M, Türkoğlu R, Akman-Demir G, Eraksoy M. Comparison of the cytokine profiles of patients with neuronal-antibody-associated central nervous system disorders. Int J Neurosci 2012;122:284-289.

43. Zeng C, Chen L, Chen B, et al. Th17 cells were recruited and accumulated in the cerebrospinal fluid and correlated with the poor prognosis of anti-NMDAR encephalitis. Acta Biochim Biophys Sin (Shanghai) 2018;50:1266-1273.

44. Filatenkov A, Richardson TE, Daoud E, et al. Persistence of parenchymal and perivascular T-cells in treatment-refractory anti-N-methyl-D-aspartate receptor encephalitis. Neuroreport 2017;28:890-895.

45. Akanuma H, Iizuka T, Abe D, et al. Paraneoplastic anti-N-methyl-D-aspartate receptor encephalitis associated with small cell lung cancer and cytotoxic T-cell-mediated pathology: Case report. Front Immunol 2022;13:952868.

46. Dao LM, Machule ML, Bacher P, et al. Decreased inflammatory cytokine production of antigen-specific CD4(+) T cells in NMDA receptor encephalitis. J Neurol 2021;268:2123-2131.

47. Walsh DA, Borges da Silva H, Beura LK, et al. The Functional Requirement for CD69 in Establishment of Resident Memory CD8(+) T Cells Varies with Tissue Location. J Immunol 2019;203:946-955.

48. Yokoi T, Murakami M, Kihara T, et al. Identification of a unique subset of tissue-resident memory CD4(+) T cells in Crohn's disease. Proc Natl Acad Sci U S A 2023;120:e2204269120.

49. Rosen SF, Soung AL, Yang W, et al. Single-cell RNA transcriptome analysis of CNS immune cells reveals CXCL16/CXCR6 as maintenance factors for tissue-resident T cells that drive synapse elimination. Genome Med 2022;14:108.

50. Wein AN, McMaster SR, Takamura S, et al. CXCR6 regulates localization of tissue-resident memory CD8 T cells to the airways. The Journal of experimental medicine 2019;216:2748-2762.

51. Lyu Y, Zhou Y, Shen J. An Overview of Tissue-Resident Memory T Cells in the Intestine: From Physiological Functions to Pathological Mechanisms. Front Immunol 2022;13:912393.

52. Kothur K, Wienholt L, Mohammad SS, et al. Utility of CSF Cytokine/Chemokines as Markers of Active Intrathecal Inflammation: Comparison of Demyelinating, Anti-NMDAR and Enteroviral Encephalitis. PLoS One 2016;11:e0161656.

53. Zhu J, Paul WE. CD4 T cells: fates, functions, and faults. Blood 2008;112:1557-1569.

54. Chen J, Ding Y, Zheng D, et al. Elevation of YKL-40 in the CSF of Anti-NMDAR Encephalitis Patients Is Associated With Poor Prognosis. Front Neurol 2018;9:727.

55. Miyamoto M, Fujita T, Kimura Y, et al. Regulated expression of a gene encoding a nuclear factor, IRF-1, that specifically binds to IFN-beta gene regulatory elements. Cell 1988;54:903-913.

56. Stark GR, Darnell JE, Jr. The JAK-STAT pathway at twenty. Immunity 2012;36:503-514.

57. Philip M, Schietinger A. CD8(+) T cell differentiation and dysfunction in cancer. Nat Rev Immunol 2021.

58. Junker A, Ivanidze J, Malotka J, et al. Multiple sclerosis: T-cell receptor expression in distinct brain regions. Brain 2007;130:2789-2799.

59. Wang P, Yao L, Luo M, et al. Single-cell transcriptome and TCR profiling reveal activated and expanded T cell populations in Parkinson's disease. Cell Discov 2021;7:52.

60. Nakagawa H, Wang L, Cantor H, Kim HJ. New Insights Into the Biology of CD8 Regulatory T Cells. Adv Immunol 2018;140:1-20.

61. Li J, Wilhelmy J, Davis MM. Characterization of KIR(+)CD8(+) Regulatory T Cells in Humans by scRNA- and TCR-seq. Methods Mol Biol 2022;2574:41-121.

62. Saligrama N, Zhao F, Sikora MJ, et al. Opposing T cell responses in experimental autoimmune encephalomyelitis. Nature 2019;572:481-487.

63. Koh JY, Shin EC. KIRs mark killers suppressing autoimmunity. Immunity 2022;55:735-737.

64. Kim HJ, Cantor H. Regulation of self-tolerance by Qa-1-restricted CD8(+) regulatory T cells. Semin Immunol 2011;23:446-452.

Figure legend

Figure 1. Single-cell transcriptomics analysis the T cell composition of cerebrospinal fluid (CSF) and periphery blood (PB). (A) Schematic representation of the study design. (B) The t-SNE plot displays 10 distinct clusters of cells, each color-coded and identified based on merged single-cell transcriptomes obtained from PB (NMDAR-E, n=4; HC, n=2) and CSF (NMDAR-E, n=3; IIH, n=6) samples. The assigned cluster names are denoted manually. (C) Expression of marker genes in T and NK cells was used to classify subclusters. The dot size indicates the percentage of cells expressing the gene, while color represents the average gene expression level per cell. (D). The t-SNE plot displayed the distribution of selected marker genes within T/NK cell subpopulation. (E) These volcano plots illustrate the comparison of CSF and PB cell subpopulations between NMDAR-E patients and controls. The plots are generated using a beta-binomial regression model and are presented as a fold change (log10) against p value (-log10). The horizontal line denotes the significance threshold. (F) Representative contour plots and summary scatter plots show the percentage of $CD45RA^{+}CCR7^{-}$ ($CD8^{+}$Temra) and $CD45RA^{-}CCR7^{-}$ ($CD8^{+}$Tem) cells in CSF from control individuals (n = 12) and NMDAR-E patients (n = 15). **$p < 0.01$, two-tailed unpaired Student's t test. (G) Representative contour plots and summary scatter plots show the percentage of $CD8^{+}$Temra, $CD45RA^{+}CCR7^{+}$($CD8^{+}$Tn), $CD45RA^{-}CCR7^{+}$ ($CD8^{+}$Tcm), and $CD8^{+}$Tem cells in PB from control individuals (n =21), acute phage NMDAR-E patients (n = 34), and relapse phage patients (n=13). **$p < 0.01$, ***$p < 0.001$, One-Way ANOVA test. Flow charts of for (F-G)

are provided in Figure e-3.

Figure 2. Transcriptomic characteristics of T cell subsets in the CSF and PB of patients with NMDAR-E patients and controls. (A) Differential gene expression (DEG) of $CD4^+$T cells and $CD8^+$T cells in the CSF of NMDAR-E patients compared to controls. Source data are provided in Table S7. (B) DEGs within T cell subclusters in the CSF of both NMDAR-E patients and control individuals, and calculated the averaged scaled expression levels across all cells within each group. (C) DEG of $CD4^+$T cells and $CD8^+$T cells in the PB of NMDAR-E patients compared to controls. Source data for are provided in Table S8. (D) DEGs within T cell subclusters in the PB of both NMDAR-E patients and control individuals, and calculated the averaged scaled expression levels across all cells within each group.

Figure 3. Significant TCR clone expansion of $CD8^+$T cells in both CSF and PB of NMDAR-E patients. (A) Distribution of clonal cells in T cell clusters found in the NMDAR-E patients (CSF, n=3; PB, n=4) and healthy controls (HC) (n=2). (B) TCRαβ clonality of T cells in CSF and PB from NMDAR-E patients, as well as blood samples from HC, represented with clones color-coded according to their proportion of total TCRαβ sequences. (C-E) Bar graphs illustrating the cellular proportions of three different clonal expansion groups in each T cell cluster, derived from PB of HC (C), PB of NMDAR-E patients (D), and CSF of NMDAR-E patients (E). (F-G) Volcano plots comparing the differential gene expression (DEGs) between highly TCR clonal (clonal TCRαβ $\geq$ 3) and unclonal T cells in both blood (F) and CSF (G) from NMDAR-E patients. Detailed source data for (F, G) are provided in Table S9. (H) Heatmaps showing selected DEGs in highly clonal (clonal TCRαβ $\geq$ 3) in PB and CSF of NMDAR-E patients, compared to unclonal T cells. Heatmap colors indicate z-scored values for mean gene expression in each group. (I-J) Sharing of expanded TCR clonotypes across T cell clusters in the PB (I) and CSF (J) of NMDAR-E patients. The bottom heatmap shows the number of shared expanded TCR clonotypes for each cluster pair in NMDAR-E patients.

Figure 4. In vitro co-culture of B cells and $CD8^+$T cells from NMDAR-E patients and controls. (A) Flow charts of flow cytometry. (B-E) Representative contour plots and summary scatter plots showing the percentage of annexin V^+ B cells (B-C) and annexin V^+ $CD8^+$T cells (D-E) at 1 day and 7 day of co-culture from PB of 6 healthy controls (HC) and 9

NMDAR-E patients. (F-I) Representative contour plots and summary scatter plots showing the percentage of annexin V^+ASCs, annexin V^+ memory B cells (Bm), annexin V^+ CD27-, annexin V^+ DN cells at 7 day of co-culture from the PB of HCs and NMDAR-E patients. * < 0.05; **P < 0.01; ***P < 0.001; evaluated using two-tailed unpaired Student's t test.

Figure 5. Changes of KIR^+CD8 T cells in NMDAR-E patients (A) Expression of KIR transcripts (KIR3DL1 and KIR2DL3) in $CD8^+$T cells from the CSF and PB of control individuals (CSF, n= 6; Blood, n=2) and NMDAR-E patients (CSF, n=3; Blood, n=4). (B) t-SNE plots showing the distribution of KIR^+CD8^+T cells (expressing KIR3DL1 and/or KIR2DL3 genes) and KIR^-CD8^+T cells in the CSF and PB of controls and NMDAR-E patients. (C) The composition of KIR^+CD8^+T cell population shown in Fig.5B. (D) Flow charts of KIR^+CD8^+T cell subclusters. (E-F) Representative contour plots and summary scatter plots show the percentage of $CD158e^+$cells in $CD8^+$T cells (E) and $CD45RA^+$cells in $CD158e^+CD8^+$T cells (KIR^+CD8^+Temra) (F) from the PB of HC (n=11) and NMDAR-E patients (mild/moderate group, n=10; severe group, n=9; relapsed group, n=13; remission group, n=8).

Figure 6. TCR clonal characteristics of KIR^+CD8^+T and their interaction with B cells. (A) t-SNE plots of KIR^+ $CD8^+$T cells from NMDAR-E patients and controls with clonal and unclonal cells annotated with different colors (clonal, red; unclonal, green). (B) TCRαβ clonality of KIR^+CD8^+T in the CSF and PB of NMDAR-E patients and PB of healthy control (HC). Clones are colored by proportion of the total TCRαβ sequences. (C-D) The differential gene expression (DEG) of expanded TCR clones revealed increased expression of cytotoxic effector genes in the clonal KIR^+CD8^+T cells of NMDAR-E patients as compared to unclonal KIR^+CD8^+T in both PB (C) and CSF (D) samples. Detailed source data for (C, D) are provided in Table S10. (E-F) Analysis of the top 10 KEGG pathways enriched for DEGs in KIR^+CD8^+T cells with and without TCR clones in the PB (E) and CSF (F) of NMDAR-E patients. (H) Cell-cell interaction analysis predicts interactions between KIR^+CD8^+T cells and KIR^- $CD8^+$T cells with plasma cells, naïve B (Bn) cells, and memory B (Bm) cells in the CSF and PB of controls and NMDAR-E patients. (I) Dot plot illustrating cell-cell interactions between KIR^+CD8^+T cells and plasma cells, Bn cells, and Bm cells based on selected cytokines and molecules calculated by CellPhoneDB.

Supplemental information

Document S1. Figures S1-S2 and Table S1-S6

Table S7. Differential expression genes of $CD4^+$T and $CD8^+$T cells in the CSF of NMDAR-E patients versus IIH.

Table S8. Differential expression genes of $CD4^+$T and $CD8^+$T in the PB of NMDAR-E patients versus healthy controls.

Table S9. Differential expression genes of clonal T cells versus unclonal T cells from NMDAR-E patients in both blood and CSF samples.

Table S10. Differential expression genes of clonal KIR^+CD8^+T cells versus unclonal KIR^+CD8^+T cells from NMDAR-E patients in both blood and CSF samples.

Table S7-S10 are provided in separate Excel spreadsheets.

Abbreviations: NMDAR=Anti-N-methyl-D-aspartate receptor; AE=autoimmune anti-NMDAR encephalitis; CBA=cell-based assay; CNS=central nervous system; CSF=cerebrospinal fluid; PBMCs=Peripheral blood mononuclear cells; PB=peripheral blood; scTCR-Seq=single-cell TCR sequencing; scRNA-seq=Single cell RNA sequencing; Temra=$CD45RA^+$ effector memory T cells; Tem=effector memory T; Tcm=central memory T; Tn=naïve T; HC=Healthy control; IIH=Idiopathic intracranial hypertension; Bm=memory B cells; Bn=naïve B cells; ASCs= Antibody-secreting cells; DN=CD27-IgD-double negative B cells; t-SNE=t-distributed neighbor embedding; MHC=Major histocompatibility complex; DEGs=Differentially expressed genes; KIRs=killer-cell immunoglobulin-like receptors;Trm= tissue-resident memory T cells.

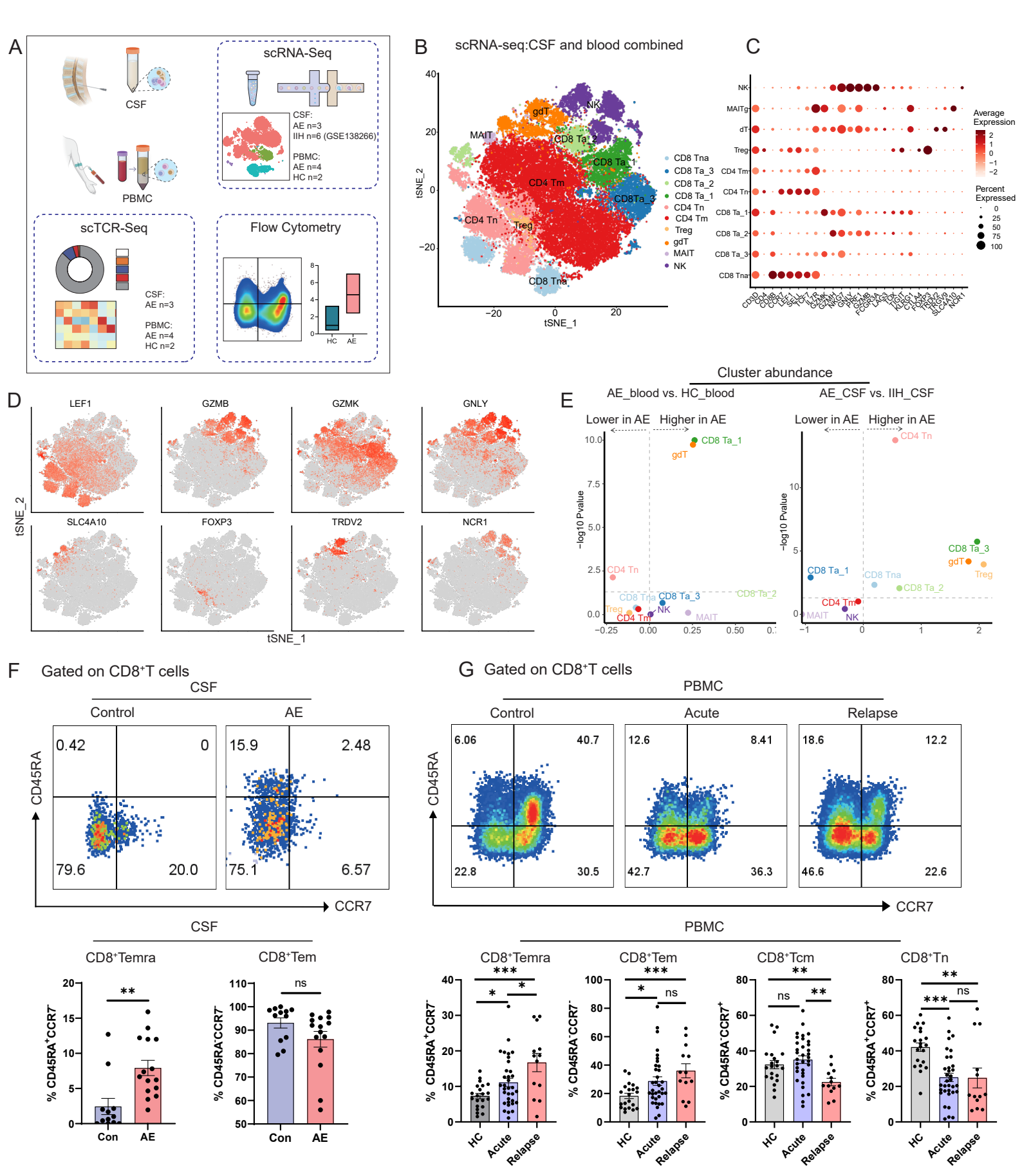
A
CSF
PBMC
scRNA-Seq
CSF:
AE n=3
IIH n=6 (GSE138266)
PBMC:
AE n=4
HC n=2
scTCR-Seq
CSF:
AE n=3
PBMC:
AE n=4
HC n=2
Flow Cytometry
HC
AE
B
scRNA-seq:CSF and blood combined
tSNE_1
tSNE_2
CD8 Tna
CD8 Ta_3
CD8 Ta_2
CD8 Ta_1
CD4 Tn
CD4 Tm
Treg
gdT
MAIT
NK
C
Average Expression
Percent Expressed
D
LEF1
GZMB
GZMK
GNLY
SLC4A10
FOXP3
TRDV2
NCR1
E
Cluster abundance
AE_blood vs. HC_blood
AE_CSF vs. IIH_CSF
Lower in AE
Higher in AE
−log10 Pvalue
F
Gated on CD8⁺T cells
CSF
Control
AE
CD45RA
CCR7
0.42
0
79.6
20.0
15.9
2.48
75.1
6.57
CD8⁺Temra
CD8⁺Tem
% CD45RA⁺CCR7⁻
% CD45RA⁻CCR7⁻
Con
AE
ns
G
Gated on CD8⁺T cells
PBMC
Control
Acute
Relapse
6.06
40.7
22.8
30.5
12.6
8.41
42.7
36.3
18.6
12.2
46.6
22.6
CD8⁺Temra
CD8⁺Tem
CD8⁺Tcm
CD8⁺Tn
HC
Acute
Relapse

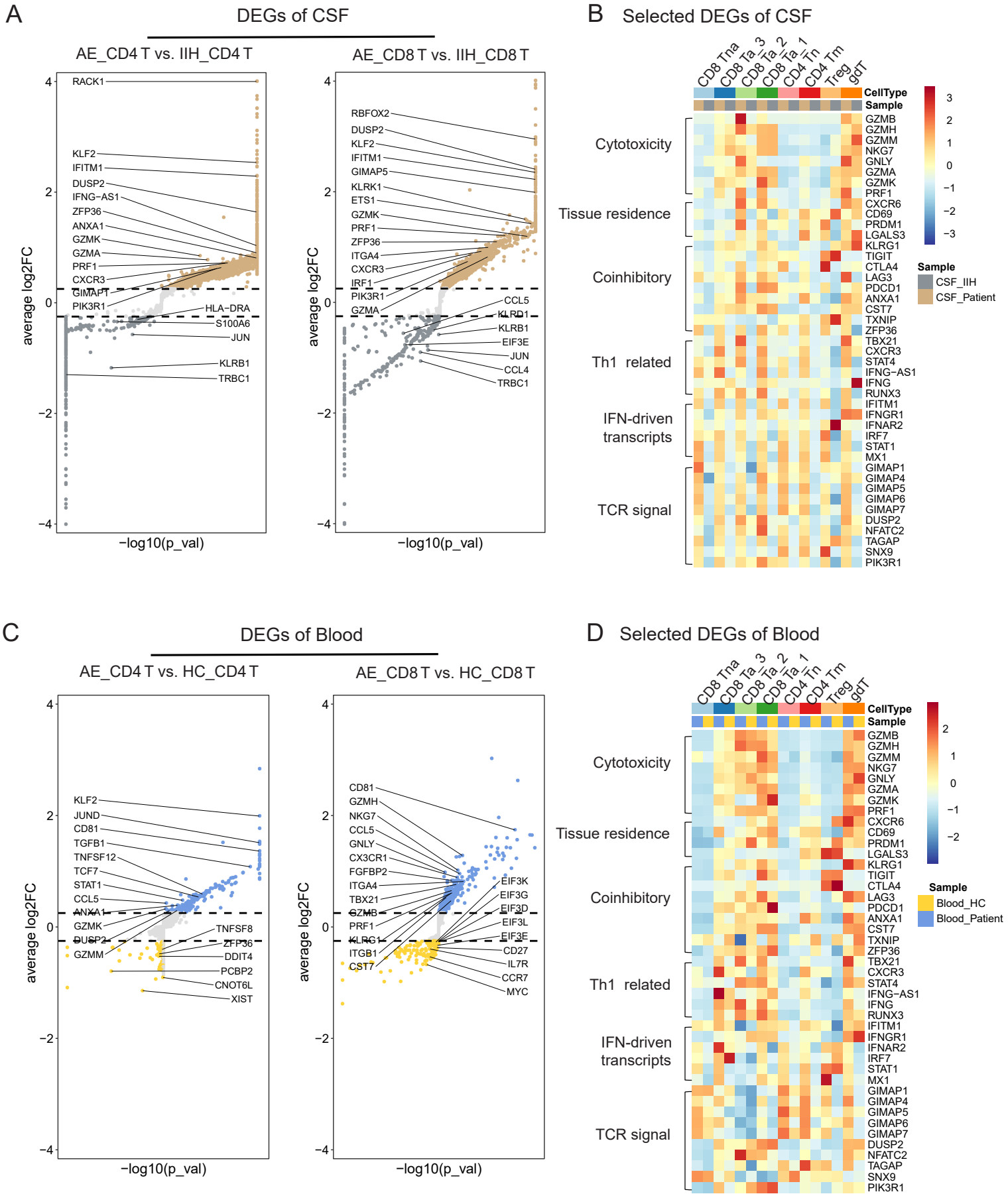
A
DEGs of CSF
AE_CD4 T vs. IIH_CD4 T
AE_CD8 T vs. IIH_CD8 T
average log2FC
−log10(p_val)
RACK1
KLF2
IFITM1
DUSP2
IFNG−AS1
ZFP36
ANXA1
GZMK
GZMA
PRF1
CXCR3
GIMAP1
PIK3R1
HLA−DRA
S100A6
JUN
KLRB1
TRBC1
RBFOX2
DUSP2
KLF2
IFITM1
GIMAP5
KLRK1
ETS1
GZMK
PRF1
ZFP36
ITGA4
CXCR3
IRF1
PIK3R1
GZMA
CCL5
KLRD1
KLRB1
EIF3E
JUN
CCL4
TRBC1
B
Selected DEGs of CSF
CD8 Tna
CD8 Ta_3
CD8 Ta_2
CD8 Ta_1
CD4 Tn
CD4 Tm
Treg
gdT
CellType
Sample
Cytotoxicity
Tissue residence
Coinhibitory
Th1 related
IFN-driven transcripts
TCR signal
GZMB
GZMH
GZMM
NKG7
GNLY
GZMA
GZMK
PRF1
CXCR6
CD69
PRDM1
LGALS3
KLRG1
TIGIT
CTLA4
LAG3
PDCD1
ANXA1
CST7
TXNIP
ZFP36
TBX21
CXCR3
STAT4
IFNG−AS1
IFNG
RUNX3
IFITM1
IFNGR1
IFNAR2
IRF7
STAT1
MX1
GIMAP1
GIMAP4
GIMAP5
GIMAP6
GIMAP7
DUSP2
NFATC2
TAGAP
SNX9
PIK3R1
Sample
CSF_IIH
CSF_Patient
C
DEGs of Blood
AE_CD4 T vs. HC_CD4 T
AE_CD8 T vs. HC_CD8 T
average log2FC
−log10(p_val)
KLF2
JUND
CD81
TGFB1
TNFSF12
TCF7
STAT1
CCL5
ANXA1
GZMK
DUSP2
GZMM
TNFSF8
ZFP36
DDIT4
PCBP2
CNOT6L
XIST
CD81
GZMH
NKG7
CCL5
GNLY
CX3CR1
FGFBP2
ITGA4
TBX21
GZMB
PRF1
KLRG1
ITGB1
CST7
EIF3K
EIF3G
EIF3D
EIF3L
EIF3E
CD27
IL7R
CCR7
MYC
D
Selected DEGs of Blood
CD8 Tna
CD8 Ta_3
CD8 Ta_2
CD8 Ta_1
CD4 Tn
CD4 Tm
Treg
gdT
CellType
Sample
Cytotoxicity
Tissue residence
Coinhibitory
Th1 related
IFN-driven transcripts
TCR signal
GZMB
GZMH
GZMM
NKG7
GNLY
GZMA
GZMK
PRF1
CXCR6
CD69
PRDM1
LGALS3
KLRG1
TIGIT
CTLA4
LAG3
PDCD1
ANXA1
CST7
TXNIP
ZFP36
TBX21
CXCR3
STAT4
IFNG−AS1
IFNG
RUNX3
IFITM1
IFNGR1
IFNAR2
IRF7
STAT1
MX1
GIMAP1
GIMAP4
GIMAP5
GIMAP6
GIMAP7
DUSP2
NFATC2
TAGAP
SNX9
PIK3R1
Sample
Blood_HC
Blood_Patient

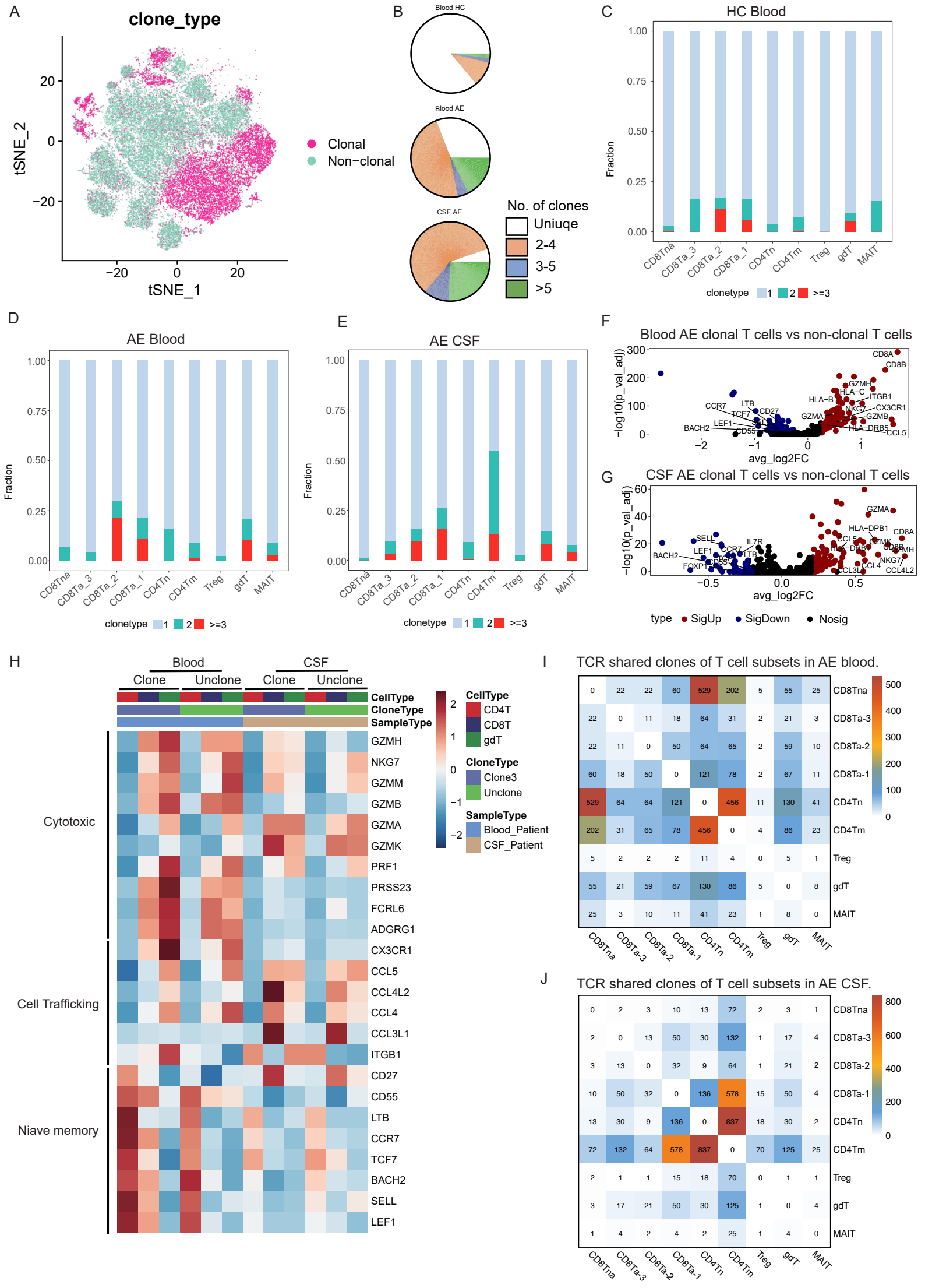
A
clone_type
tSNE_2
tSNE_1
Clonal
Non−clonal
B
Blood HC
Blood AE
CSF AE
No. of clones
Uniuqe
2-4
3-5
>5
C
HC Blood
Fraction
clonetype 1 2 >=3
D
AE Blood
E
AE CSF
F
Blood AE clonal T cells vs non-clonal T cells
−log10(p_val_adj)
avg_log2FC
G
CSF AE clonal T cells vs non-clonal T cells
type SigUp SigDown Nosig
H
Blood
CSF
Clone
Unclone
CellType
CloneType
SampleType
CD4T
CD8T
gdT
Clone3
Unclone
Blood_Patient
CSF_Patient
Cytotoxic
Cell Trafficking
Niave memory
GZMH
NKG7
GZMM
GZMB
GZMA
GZMK
PRF1
PRSS23
FCRL6
ADGRG1
CX3CR1
CCL5
CCL4L2
CCL4
CCL3L1
ITGB1
CD27
CD55
LTB
CCR7
TCF7
BACH2
SELL
LEF1
I
TCR shared clones of T cell subsets in AE blood.
J
TCR shared clones of T cell subsets in AE CSF.
CD8Tna
CD8Ta-3
CD8Ta-2
CD8Ta-1
CD4Tn
CD4Tm
Treg
gdT
MAIT

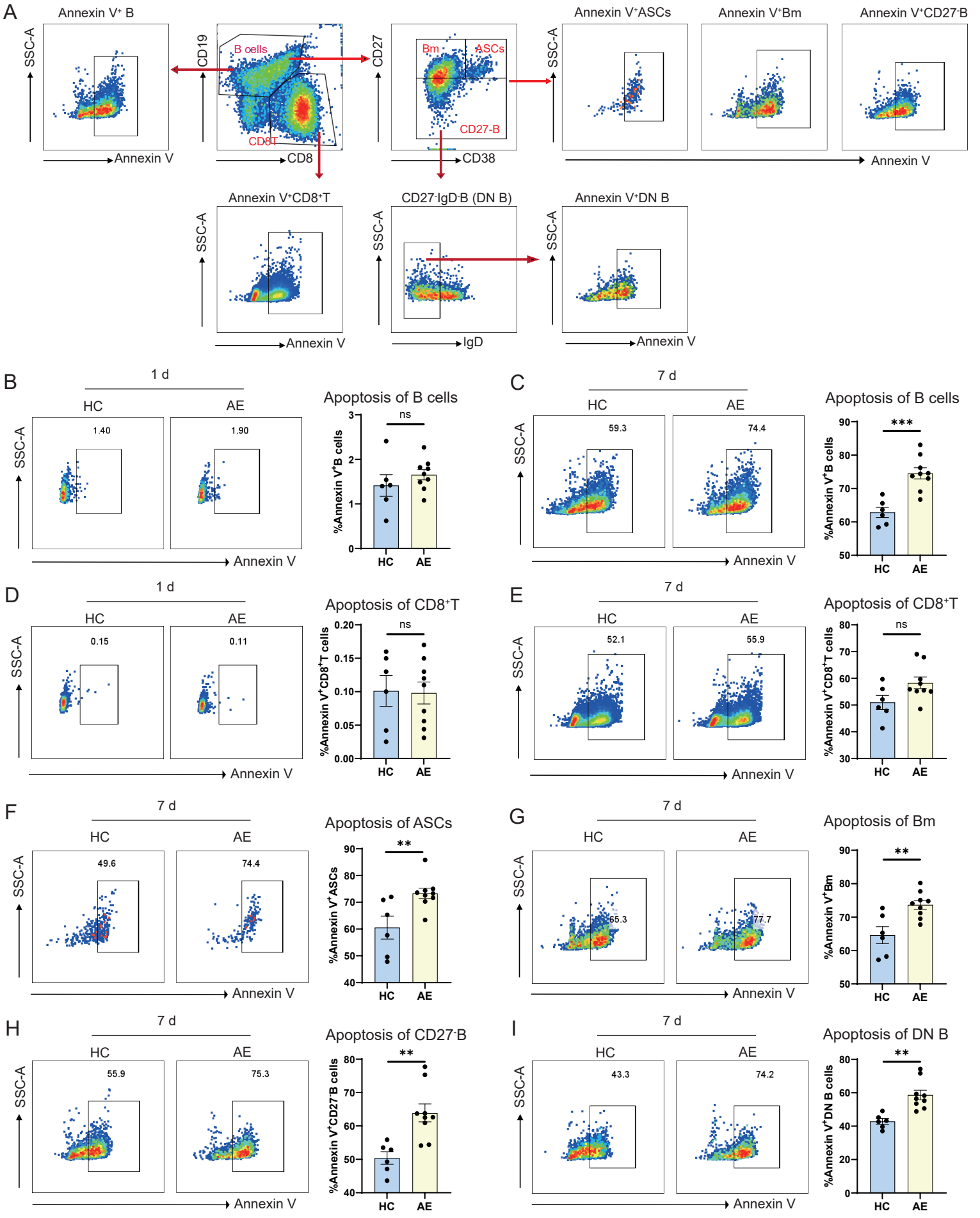
A
Annexin V+ B
SSC-A
Annexin V
CD19
B cells
CD8+T
CD8
CD27
Bm
ASCs
CD27-B
CD38
Annexin V+ASCs
Annexin V+Bm
Annexin V+CD27-B
Annexin V+CD8+T
CD27-IgD-B (DN B)
IgD
Annexin V+DN B
B
1 d
HC
AE
1.40
1.90
Apoptosis of B cells
ns
%Annexin V+B cells
C
7 d
59.3
74.4
***
D
0.15
0.11
Apoptosis of CD8+T
%Annexin V+CD8+T cells
E
52.1
55.9
F
49.6
74.4
Apoptosis of ASCs
**
%Annexin V+ASCs
G
65.3
77.7
Apoptosis of Bm
%Annexin V+Bm
H
55.9
75.3
Apoptosis of CD27-B
%Annexin V+CD27-B cells
I
43.3
74.2
Apoptosis of DN B
%Annexin V+DN B cells

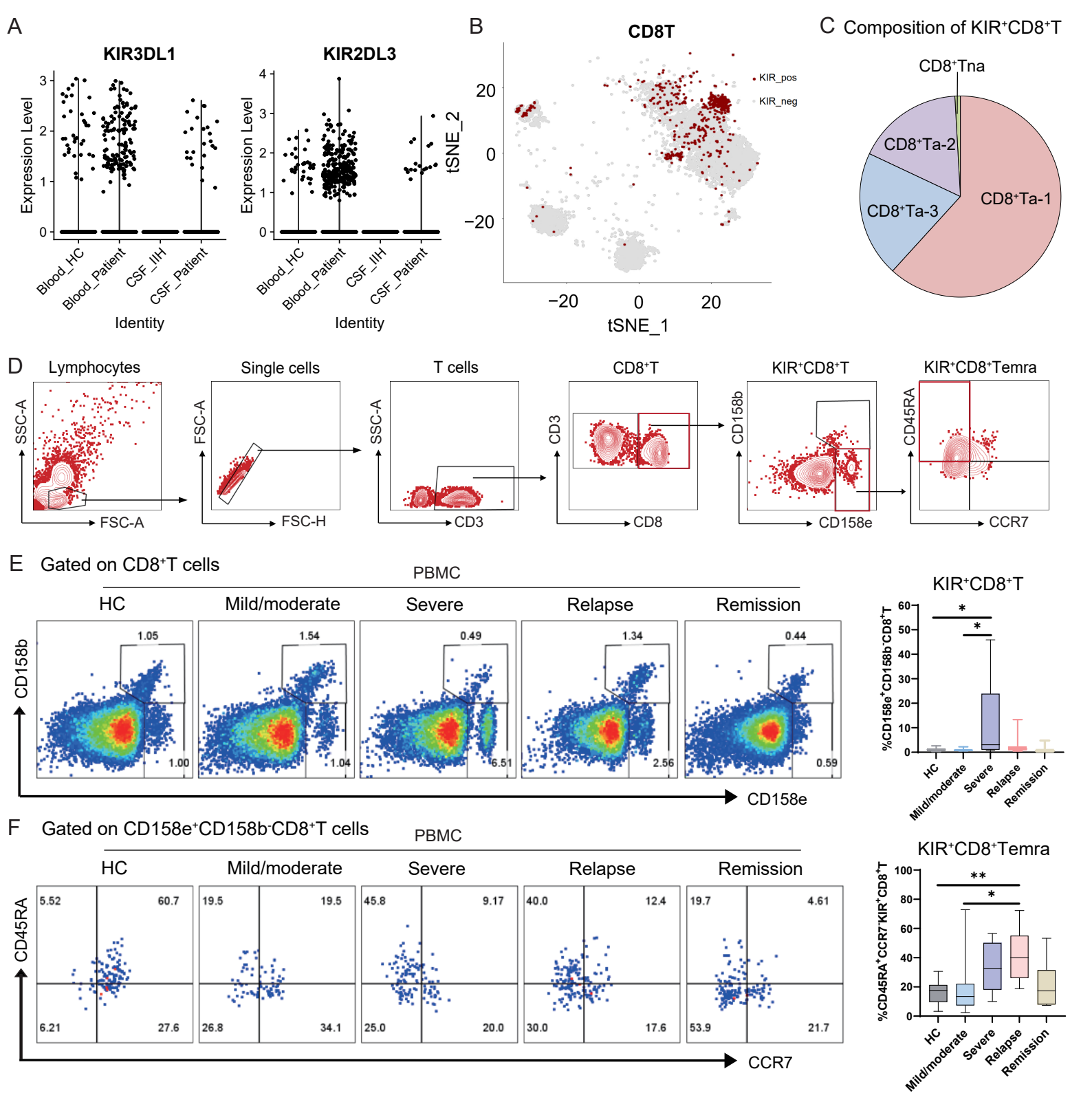
A
KIR3DL1
KIR2DL3
Expression Level
Blood_HC
Blood_Patient
CSF_IIH
CSF_Patient
Identity
B
CD8T
KIR_pos
KIR_neg
tSNE_1
tSNE_2
C Composition of KIR+CD8+T
CD8+Tna
CD8+Ta-2
CD8+Ta-3
CD8+Ta-1
D
Lymphocytes
Single cells
T cells
CD8+T
KIR+CD8+T
KIR+CD8+Temra
SSC-A
FSC-A
FSC-H
CD3
CD8
CD158b
CD158e
CD45RA
CCR7
E Gated on CD8+T cells
PBMC
HC
Mild/moderate
Severe
Relapse
Remission
1.05
1.00
1.54
1.04
0.49
6.51
1.34
2.56
0.44
0.59
KIR+CD8+T
%CD158e+CD158b-CD8+T
F Gated on CD158e+CD158b-CD8+T cells
5.52
60.7
6.21
27.6
19.5
19.5
26.8
34.1
45.8
9.17
25.0
20.0
40.0
12.4
30.0
17.6
19.7
4.61
53.9
21.7
KIR+CD8+Temra
%CD45RA+CCR7-KIR+CD8+T

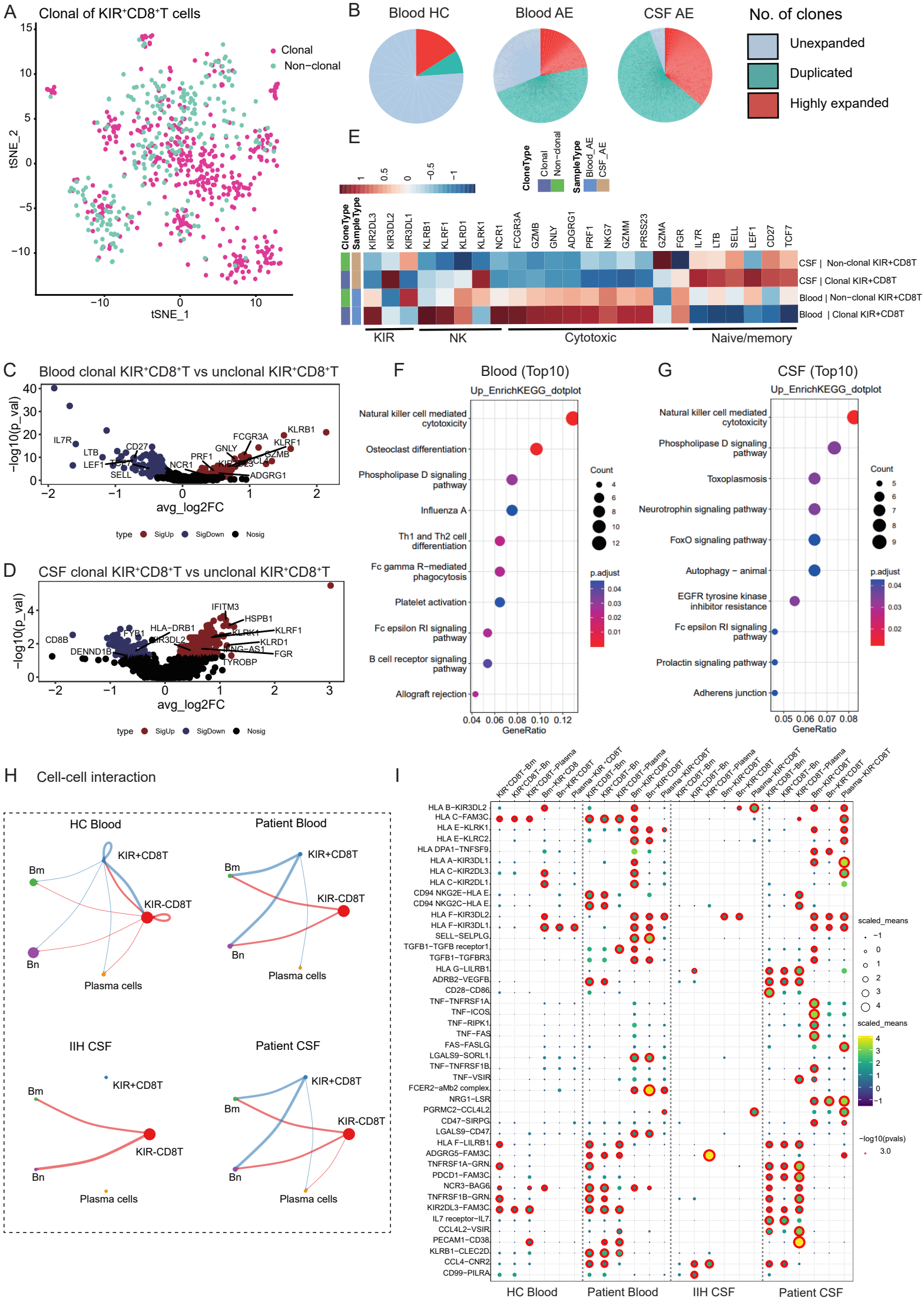
A
Clonal of KIR+CD8+T cells
Clonal
Non−clonal
tSNE_2
tSNE_1
B
Blood HC
Blood AE
CSF AE
No. of clones
Unexpanded
Duplicated
Highly expanded
E
CloneType
SampleType
Clonal
Non−clonal
Blood_AE
CSF_AE
KIR2DL3
KIR3DL2
KIR3DL1
KLRB1
KLRF1
KLRD1
KLRK1
NCR1
FCGR3A
GZMB
GNLY
ADGRG1
PRF1
NKG7
GZMM
PRSS23
GZMA
FGR
IL7R
LTB
SELL
LEF1
CD27
TCF7
CSF | Non-clonal KIR+CD8T
CSF | Clonal KIR+CD8T
Blood | Non−clonal KIR+CD8T
Blood | Clonal KIR+CD8T
KIR
NK
Cytotoxic
Naive/memory
C
Blood clonal KIR+CD8+T vs unclonal KIR+CD8+T
−log10(p_val)
avg_log2FC
type
SigUp
SigDown
Nosig
D
CSF clonal KIR+CD8+T vs unclonal KIR+CD8+T
IFITM3
HSPB1
HLA−DRB1
KLRF1
KLRD1
FGR
TYROBP
CD8B
FYB1
DENND1B
F
Blood (Top10)
Up_EnrichKEGG_dotplot
Natural killer cell mediated cytotoxicity
Osteoclast differentiation
Phospholipase D signaling pathway
Influenza A
Th1 and Th2 cell differentiation
Fc gamma R−mediated phagocytosis
Platelet activation
Fc epsilon RI signaling pathway
B cell receptor signaling pathway
Allograft rejection
Count
p.adjust
GeneRatio
G
CSF (Top10)
Up_EnrichKEGG_dotplot
Natural killer cell mediated cytotoxicity
Phospholipase D signaling pathway
Toxoplasmosis
Neurotrophin signaling pathway
FoxO signaling pathway
Autophagy − animal
EGFR tyrosine kinase inhibitor resistance
Fc epsilon RI signaling pathway
Prolactin signaling pathway
Adherens junction
Count
p.adjust
GeneRatio
H
Cell-cell interaction
HC Blood
Patient Blood
IIH CSF
Patient CSF
KIR+CD8T
KIR-CD8T
Bm
Bn
Plasma cells
I
HLA B−KIR3DL2
HLA C−FAM3C
HLA E−KLRK1
HLA E−KLRC2
HLA DPA1−TNFSF9
HLA A−KIR3DL1
HLA C−KIR2DL3
HLA C−KIR2DL1
CD94 NKG2E−HLA E
CD94 NKG2C−HLA E
HLA F−KIR3DL2
HLA F−KIR3DL1
SELL−SELPLG
TGFB1−TGFB receptor1
TGFB1−TGFBR3
HLA G−LILRB1
ADRB2−VEGFB
CD28−CD86
TNF−TNFRSF1A
TNF−ICOS
TNF−RIPK1
TNF−FAS
FAS−FASLG
LGALS9−SORL1
TNF−TNFRSF1B
TNF−VSIR
FCER2−aMb2 complex
NRG1−LSR
PGRMC2−CCL4L2
CD47−SIRPG
LGALS9−CD47
HLA F−LILRB1
ADGRG5−FAM3C
TNFRSF1A−GRN
PDCD1−FAM3C
NCR3−BAG6
TNFRSF1B−GRN
KIR2DL3−FAM3C
IL7 receptor−IL7
CCL4L2−VSIR
PECAM1−CD38
KLRB1−CLEC2D
CCL4−CNR2
CD99−PILRA
scaled_means
−log10(pvals)
HC Blood
Patient Blood
IIH CSF
Patient CSF